Selective Wireless Power Transmission Through High-Q Flat Waveguide-Ring Resonator on 2-D Waveguide Sheet

Akihito Noda, *Student Member, IEEE*, and Hiroyuki Shinoda, *Member, IEEE*

***Abstract*—2-D waveguide power transmission (2DWPT) can potentially provide a safe and wireless means of electricity transfer. Our goal is to develop a 2DWPT system in which the power is transferred only to special receiver devices and not to other objects. For this purpose, a new high-quality (high-Q) factor receiver coupler is designed, while the Q of other general objects are reduced by a thick insulator layer on the sheet. This contrast in Q enables selective power transmission to the receiver coupler. The coupler forms a flat waveguide-ring resonator together with the insulator layer. Full-wave simulations validate the difference of power extraction between the proposed coupler and flat conductor plate resonators as a standard reference of general objects. The performance of the fabricated coupler is also examined on a large open-edged sheet where a standing wave is generated, as well as on a narrow strip-shaped sheet where the standing wave is eliminated. In the case where eight 50-Ω loaded couplers operate on a 90 cm × 60 cm large waveguide sheet simultaneously, the total microwave transmission efficiency achieved 87.7%.**

***Index Terms*—Electromagnetic (EM) compatibility, energy confining structure, resonant coupler, 2-D waveguide, waveguide-ring resonator (WRR), wireless power transmission (WPT).**

I. Introduction

SELECTIVITY along with efficiency is one of the most important factors in wireless power transmission (WPT) used in general environments where the target device, extraneous objects, and human bodies coexist. The selectivity can be evaluated from two aspects: electromagnetic (EM) power absorption and EM field generation. From the former point of view, the EM power should be selectively absorbed only by the target device and not by other objects. For the latter, the significant EM field should be generated only inside the transmitter, receiver, and power transmission medium, where the other object cannot touch, and should not leak outside them. General-environment WPT systems must satisfy not only the former requirement, but also the latter one, because the strong EM field can have interactions with human bodies and can damage electrically sensitive devices, even if the absorbed power is acceptable. The WPT system proposed in this paper has selectivity in both the aspects, using the 2-D waveguide power transmission (2DWPT) scheme [1]–[3], as shown in Fig. 1.

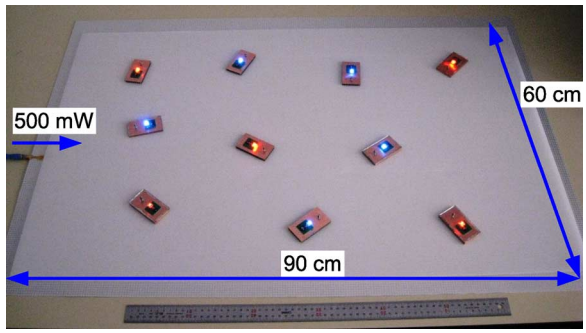

Fig. 1. 2-D power transmission demonstration. Ten LED-loaded waveguide-ring resonator (WRR) couplers are operating on the 2-D waveguide sheet covered with a 4-mm-thick insulator layer, while 500-mW power of 2.45-GHz microwave is fed into the sheet. The power consumption of each LED is estimated to be a few tens of milliwatts. The dimensions of the sheet and the coupler are 90 cm × 60 cm and 6.4 cm × 3.6 cm, respectively. The ruler in front of the sheet, just for scale, is 60-cm long.

WPT includes two types: long-range remote WPT and close-range proximity WPT. The former system can be realized by using EM radiation [4]–[6] or resonant inductive coupling [7]. By using resonant coupling, significant power can be transferred to the resonant receiver with low power absorption by off-resonant objects around there. However, the resonant transmitter and receiver generate strong EM field around themselves and can induce a strong electromotive force along a conductor loop (e.g., coiled headphone cable, necklace, circuit board pattern in electronic appliances, etc.) surrounding the magnetic field.

The latter one, i.e., close-range proximity WPT, can be a reasonable solution to reduce such a risk and to improve the selectivity, if the users can compromise on the freedom in the receiver position. Sheet-like WPT media can enhance the freedom in the receiver position into 2-D area, requiring the close proximity between the medium and receiver. Although the geometrical restriction can be a drawback, the scheme is applicable to many power-consuming items that are put on planes such as desks, floors, walls, and ceilings.

A switchable coil array [8], [9] is one realization of that scheme. In order to cover a larger area than each coil size, the system requires numbers of coils, switches, and drivers, therefore the coil array become complex and costly.

Manuscript received February 23, 2011; accepted May 03, 2011. Date of publication June 13, 2011; date of current version August 17, 2011. This work was supported in part by the National Institute of Information and Communications Technology (NICT) 13701. The work of A. Noda was supported under a Grant-in-Aid for JSPS Fellows (22·6659).

The authors are with the Department of Information Physics and Computing, University of Tokyo, Tokyo 113-8656, Japan (e-mail: Akihito_Noda@ipc.i.u-tokyo.ac.jp; shino@alab.t.u-tokyo.ac.jp).

Color versions of one or more of the figures in this paper are available online at http://ieeexplore.ieee.org.

Digital Object Identifier 10.1109/TMTT.2011.2156425

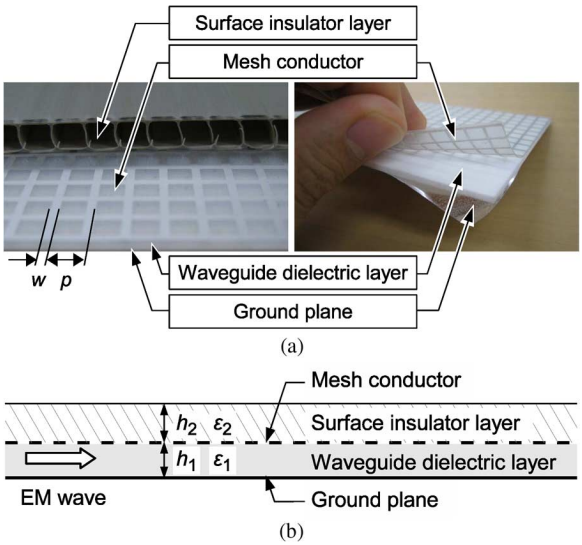

Fig. 2. (a) Sheet consists of three layers: ground conductor plane, dielectric layer, and mesh conductor plane. The mesh pitch p and linewidth w determine the sheet surface reactance. Additionally, the sheet is covered by a thick surface insulator layer in this study. (b) Cross section of the sheet and definitions of design parameters.

The 2DWPT employed in this study is another realization, based on microwave propagation along a sheet-like waveguide [1]. The system can potentially achieve a high-selectivity and large-area WPT with a simple passive medium. The microwave power (a 2.4–2.5-GHz industrial, scientific, and medical (ISM) band is used in this study) guided by the sheet can be extracted by special receiver couplers on the sheet. The waveguide is a simple dielectric sheet sandwiched by two conductor planes, as shown in Fig. 2, and can be produced at low cost. The system can also support converging beam power transmission to a small receiver on a large passive waveguide sheet without any active switching element in the sheet [10]. A similar system that uses another type of waveguide sheet [11] has been also proposed. In those preceding studies on 2DWPT, however, the selectivity and transfer efficiency had not been evaluated quantitatively.

The sheet upper side conductor, which serves as the interface of the power transmission, is mesh patterned and generates evanescent EM field above the mesh [1]. The linewidth and the pitch of the periodical mesh pattern determine the evanescent field intensity outside the sheet for the unit power density flowing along the sheet. Since the strong EM field above the mesh decays steeply with respect to the distance from the surface, the EM exposure of objects on the sheet is reduced by covering the sheet with a thick insulator layer.

The objective of this paper is to establish a procedure for designing a selective 2DWPT system. This paper contains three unpublished contents, which are: 1) a theory on the underlying principle to support the procedure; 2) a proposal of a new-type of coupler to embody the principle; and 3) a trial power transmission experiment to demonstrate the practicability of the prototype system. The presented theory clarifies the essence of our previous analyses shown in the conference proceedings [3], [12]. The proposed coupler is simpler and more efficient than our previous devices. We demonstrate the practicability of the system through a trial power transmission experiment. In the case where eight 50-Ω loaded couplers operate on a 90 cm $\times$ 60 cm large waveguide sheet simultaneously, the total microwave transmission efficiency without taking account of rectifying efficiency achieved 87.7% at a maximum.

To evaluate the selectivity, we compare the power extraction out of the sheet by the coupler and that by various sizes of flat conductor plates, as introduced in our previous study [12]. The latter is a standard reference of unwanted power extraction by extraneous objects. This evaluation is stricter and more reasonable than the evaluation of specific absorption rate (SAR) [13] for a human tissue directly touching on the sheet surface because the resonant conductor can extract much larger power than the lossy dielectric tissue, as described in Section II. One selectivity measure is defined as the ratio of the power that can be extracted by the receiver coupler to that by the flat conductor plate.

This paper is organized as follows. In Section II, we review an analysis on the relationship between the power extracted from the sheet and the EM field around the sheet surface [3]. Based on the relationship, Section III describes the principle of selectivity improvement. Section IV presents the simulation result of the evaluation on unwanted power extraction by the flat conductor plate. Section V shows the simulation results of receiver coupler operation. In Section VI, the basic performance of the coupler is validated experimentally. Section VII presents a experiment where microwave power is transferred to plural couplers operating on a large sheet simultaneously and proves the feasibility of a high-efficiency 2DWPT system. Section VIII presents a conclusion.

II. Power Extraction Across Mesh Conductor

In this section, we describe a relationship between the EM field distribution and the power extracted from the sheet across the mesh conductor layer. The conclusion presented here is partly based on the analysis in our previous work [3].

Here we consider a 2-D problem in which an arbitrary object is put on the waveguide sheet, as shown in Fig. 3(a). Although the 2-D models in Fig. 3 represent only a certain cross section of the sheet and objects, they help us to understand the power extraction principle.

We suppose that an EM wave with angular frequency ω fed into the sheet travels in the $+x$-direction and that only the TM field invariant in the y-direction exists in the model. H_L^y and H_U^y are the complex amplitudes of the y-components of the magnetic fields on the lower $(-z)$ side and on the upper $(+z)$ side of the mesh plane, respectively. We assume that the thickness of each layer of the sheet is significantly smaller than the EM wavelength in the sheet and that the magnetic field is uniform in the z-direction in each layer. We also assume that the mesh pitch is sufficiently smaller than the wavelength, thus our terms of current and EM field denote the spatial averages of them over the mesh period.

We consider a rectangular area $ABCD$ that is bounded by the object base and mesh plane, as shown in Fig. 3(a). The power flowing out of the sheet across $\overline{AB}$ on the mesh plane is denoted by P_{AB} and is calculated as follows [3]:

$$P_{AB} = \frac{X_O}{2} \int_{\overline{AB}} |H_U^y| \, |H_L^y| \sin\theta \, dx \tag{1}$$

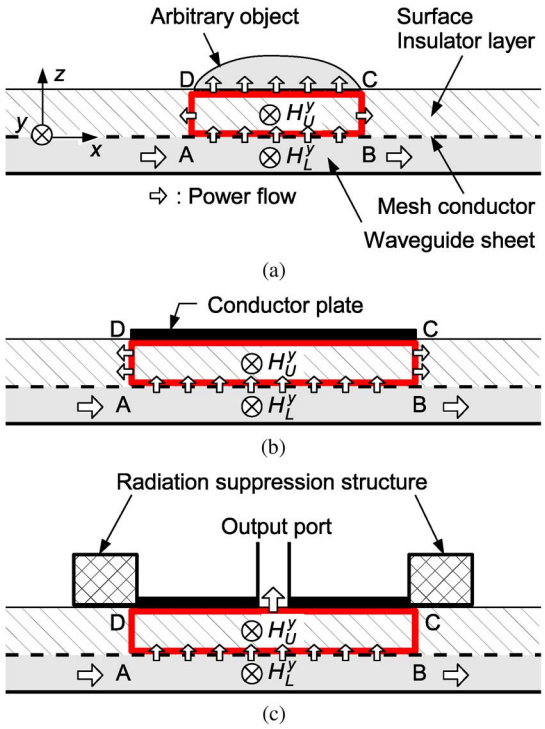

Fig. 3. (a) Cross-sectional model of a waveguide sheet. (b) Flat ideal conductor plate is put on the sheet. (c) Coupler with a radiation suppression structure is put on the sheet. Suppose that only the TM field travels in the models.

where θ and X_O are the phase difference between H_U^y and H_L^y, and surface reactance of the mesh conductor plane, respectively,

$$\theta \equiv \arg H_U^y - \arg H_L^y \tag{2}$$

$$X_O \equiv \mathrm{Im}\left[E_O^x / I_O^x\right]. \tag{3}$$

E_O^x and I_O^x denote the x-components of the electric field and current density at the mesh conductor plane, respectively. $\mathrm{Im}[\cdot]$ represents taking the imaginary part of the function in the square brackets. Surface reactance X_O is a constant determined by the geometrical mesh pattern.

The power extracted from the sheet, P_{AB}, is divided into four components as follows:

$$P_{AB} = P_{BC} + P_{CD} + P_{DA} + P_{\mathrm{dis}} \tag{4}$$

where P_{dis} represents the power dissipated inside $ABCD$ due to the lossy materials. Hereafter, we neglect P_{dis} for simplicity. P_{CD}, the power flowing out of the cavity through $\overline{CD}$, is absorbed by the object on the insulator layer. P_{BC} and P_{DA}, respectively, are the power flow outward from the cavity across $\overline{BC}$ and $\overline{DA}$ radiated into the space.

Here we define two classes of the objects: "an extraneous object" and "an energy confinement (EC) coupler."

The former is an object other than the target of power transmission and can be a resonator, but without the EC structure. Extraneous objects are required to avoid significant power extraction P_{AB}. It means that the radiation P_{BC} and P_{DA} should be small, as well as the absorption P_{CD}. We consider various sizes of conductor plates as a standard reference of the extraneous object, as shown in Fig. 3(b), since they seem the worst EM absorbers found in our daily life when they are at their resonant states. The absorption by human bodies directly touching the sheet surface is less than the resonant-plate absorption, as described below.

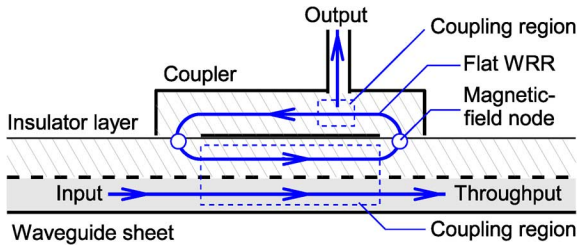

Fig. 4. Cross-sectional view of a 2-D waveguide sheet and an EC coupler. The insulator layer covering the sheet and the coupler form a flat WRR. The perimeter of the WRR is one wavelength and the coupler length in x-direction is a half wavelength. The resonant mode has the magnetic-field nodes at both ends of the coupler.

The latter, an EC coupler, is a high-Q resonant coupler enclosed with a radiation suppression structure for efficient power extraction. It strongly confines EM energy inside the resonant cavity area $ABCD$ by reducing the radiation loss, as shown in Fig. 3(c). The coupler should attain both high power absorption P_{CD} and high internal efficiency η_{int} that is defined as

$$\eta_{\mathrm{int}} \equiv P_{CD}/P_{AB}. \tag{5}$$

One example of the radiation suppression structures is a mushroom-type electromagnetic bandgap (EBG) structure that serves as an electric wall (short end) [3], [14], and another one is a $\lambda/4$-choke structure that serves as a magnetic wall (open end) [12]. In this paper, we propose to use a WRR [15] as the EC structure. A schematic illustration of the coupler is shown in Fig. 4. When the receiver coupler touches the sheet surface, they form a flat WRR that is excited through the mesh plane of the sheet. Its boundary condition at the coupler ends is high-impedance open-end, the same as that of the $\lambda/4$-choke. The structure is simple and is significantly reduced in volume compared to the vertical choke structure [12].

In the following section, we discuss how to decrease P_{AB} for extraneous objects and how to increase P_{CD} for the EC coupler.

III. Design Basis of Sheet and Coupler

A. Selectivity From Quality Factor

One aspect of selectivity is quantified by selectivity factor, which is defined as the ratio of P_{CD} for the EC coupler to P_{AB} for an extraneous object. Maximizing the selectivity factor is roughly equivalent to maximizing the ratio of the Q factor of the resonant cavity for the EC coupler to that for the extraneous object, as described below.

Here we define the Q factor of the cavity, Q_C, at resonance as follows:

$$Q_C \equiv \omega_0 W_m / P_{AB} \tag{6}$$

where ω_0 is the resonant angular frequency and W_m denotes the magnetic field energy stored in the cavity

$$W_m \equiv \frac{\mu_0}{2} \iint_{ABCD} |H_U^y|^2 \, dxdz \tag{7}$$

with an assumption that the permeability of the insulator layer is equal to that of the atmosphere, μ_0. In a rough estimation assuming the spatial constancy of $|H_U^y|$ in $ABCD$ area, both Q_C and P_{AB} are proportional to $|H_U^y|$ since W_m and P_{AB} on the right-hand side of (6) are, respectively, a second- and first-order function of $|H_U^y|$, as derived from (7) and (1), respectively. Therefore, increasing P_{AB}, Q_C, and $|H_U^y|$ are roughly all equivalent among them. Thus, our goal is to increase Q_C for the EC coupler and to reduce that for the extraneous object.

In order to reduce Q_C for any extraneous objects, a controllable factor is the radiation Q, which is defined as

$$Q_{\rm rad} \equiv \omega_0 W_m/(P_{BC}+P_{DA}). \tag{8}$$

Additionally, by defining the external Q as

$$Q_{\rm ext} \equiv \omega_0 W_m/P_{CD} \tag{9}$$

Q_C is expressed as

$$Q_C^{-1} = Q_{\rm rad}^{-1} + Q_{\rm ext}^{-1}. \tag{10}$$

This relationship gives us the following suggestions. In order to reduce P_{AB} for general objects, it is effective to increase the thickness of the surface insulator layer, which decreases Q_C by decreasing $Q_{\rm rad}$. In the case that the material touching at $\overline{CD}$ is a lossy conductor or a dielectric, P_{AB} further decreases because of the lower Q_C.

On the other hand, $Q_{\rm rad}$ should be high for the EC coupler to have a large P_{AB} as a necessary condition for significant power absorption P_{CD}. As shown in Section III-B, it is possible to find an EC coupler structure having a high $Q_{\rm rad}$ for a thick surface insulator layer. $Q_{\rm ext}$ is tuned properly for maximizing P_{CD} or $\eta_{\rm int}$.

B. Countermeasure Against Large Objects

The extracted power P_{AB} also depends on the length of $\overline{AB}$. In order to reduce power extraction by large conductor plates, the significant difference in permittivity between the waveguide layer and the surface insulator layer is required.

The permittivity determines the wavelengths of EM waves in the materials. If a certain difference exists between the wavelength in the waveguide layer and that in the surface insulator layer, then $\sin\theta$ in (1) oscillates between positive and negative along x. The larger difference results in the shorter period of $\sin\theta$ and the smaller P_{AB}. Thus, the significant permittivity difference prevents the power extraction P_{AB} even for a large $\overline{AB}$.

In order to confine most of the EM wave energy inside the waveguide layer, $\varepsilon_2 < \varepsilon_1$ is required because $\varepsilon_2 > \varepsilon_1$ can cause leaky waves outward from the waveguide. Thus, we should choose materials with low and high permittivities for the surface insulator layer and the waveguide dielectric layer, respectively.

In the following sections, we show an example of the proposed system in which practical selectivity is realized. The parameters of the sheet and coupler were obtained in trial and error for showing the existence proof of the selective power transmission.

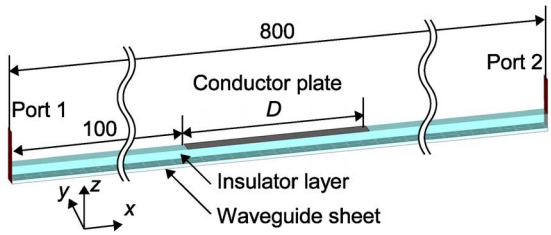

Fig. 5. Simulation model where the conductive plate touches the surface insulator layer. The models have narrow width (4 mm) for y-axis. The $\pm y$ boundary conditions are magnetic wall. Thus, the model simulates that the quasi-plane wave propagates along x-axis in the infinitely periodic sheet structure with respect to y-axis. Various length of conductor plates are simulated to estimate the worst case radiation.

TABLE I
SHEET DESIGN PARAMETERS

Symbol	Value	Description
ε_1	2.1	Relative permittivity of waveguide layer
ε_2	1.17	Relative permittivity of surface insulator layer
h_1	1.0 mm	Thickness of waveguide layer
h_2	4.0 mm	Thickness of surface insulator layer
p	4.0 mm	Mesh conductor pitch
w	1.0 mm	Mesh conductor line width

IV. FULL-WAVE SIMULATION ON EXTRACTION BY CONDUCTOR PLATE

We evaluate the power extraction by various sizes of ideal conductor plates touching the sheet through computer simulations. The test can evaluate the worst case (maximum) of extraction by a flat surface consisting of a homogeneous material put on the sheet.

The simulation model is shown in Fig. 5. Although this model represents only a narrow segment of the sheet and the object, it helps us to verify our concept.

The scattering parameters (S-parameters) are calculated through 3-D full-wave simulations using CST Microwave Studio. The extracted power ratio $p_{\rm ext}$ by the conductor plate is defined and calculated as follows:

$$p_{\rm ext} \equiv \frac{P_{\rm ext}}{P_{\rm sup}} = p_0 - \left(|S_{11}|^2 + |S_{21}|^2\right) \tag{11}$$

where $P_{\rm sup}$ and $P_{\rm ext}$, respectively, represent the supplied power into the sheet and the extracted power out of the sheet due to the conductor plate. S_{11} and S_{21} are, respectively, the reflectance at port 1, which is set at the $-x$ end of the sheet, and the transmittance from port 1 to port 2, which is set at the $+x$ end of the sheet, as shown in Fig. 5. A parameter p_0 represents $|S_{11}|^2 + |S_{21}|^2$ for the simulation model without the conductor plate. Due to the lossy material of the mesh conductor (assuming aluminum), p_0 is slightly less than 1.0.

We designed the sheet parameters, as shown in Table I. These are chosen from several available materials. The symbols shown in the table correspond to those in Fig. 2. On the basis described in Section III-B, we designed the sheet so that the relative permittivity of the waveguide layer $\varepsilon_1 = 2.1$ is significantly larger than that of the surface insulator layer $\varepsilon_2 = 1.17$ and so that the surface insulator layer is significantly thick. The insulator

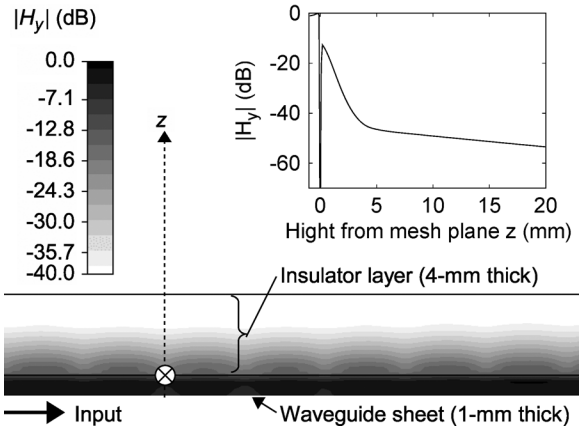

Fig. 6. Simulated magnetic field $|H_y|$ distribution map. The inset shows the $|H_y(z)|$ in decibels (the maximum $|H_y|$ in the waveguide dielectric layer is set to 0 dB) along the vertical dashed line. $|H_y|$ steeply decays to less than -40 dB by $z = 4$ mm, the insulator layer surface. Note that $|H_y|$ is zero at $z = 0$ due to the mesh conductor with finite thickness (0.01 mm).

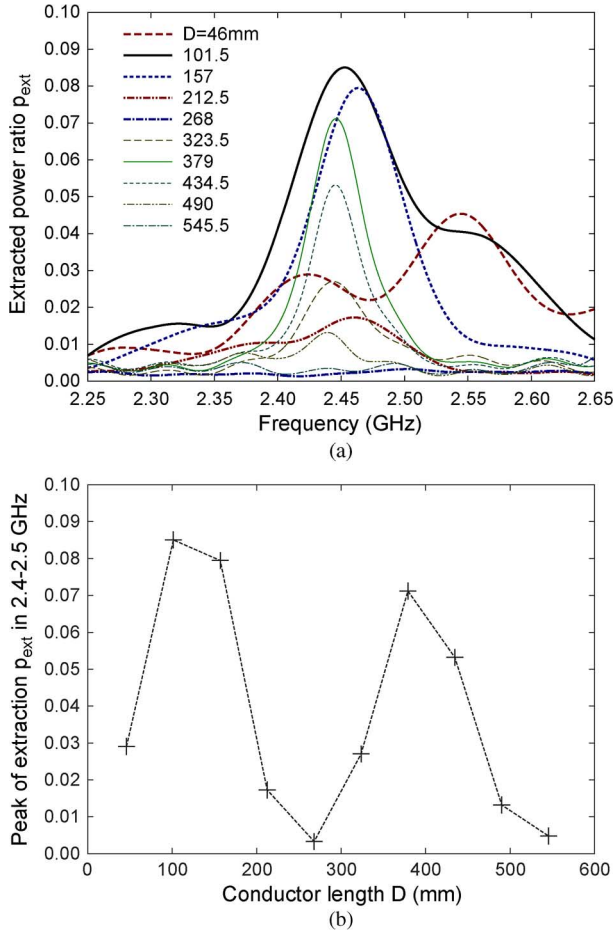

Fig. 7. (a) Extracted power by the conductor plates with length $D = 46 + 55.5n$ mm where $n = 0, 1, \ldots, 9$. All of them have a peak near 2.5 GHz. The peak value is nearly equal to or less than 8.5%. (b) Peak value in 2.4-2.5 GHz versus the plate length. The dashed lines connecting data points are for eye guide. The peak does not monotonically increase with the conductor length.

layer thickness $h_2 = 4.0$ mm is much larger than that in our previous studies (0.05–0.25 mm). The evanescent field above the mesh surface has two components: one is relatively large, comparable to the EM field inside the sheet, and steeply decays;

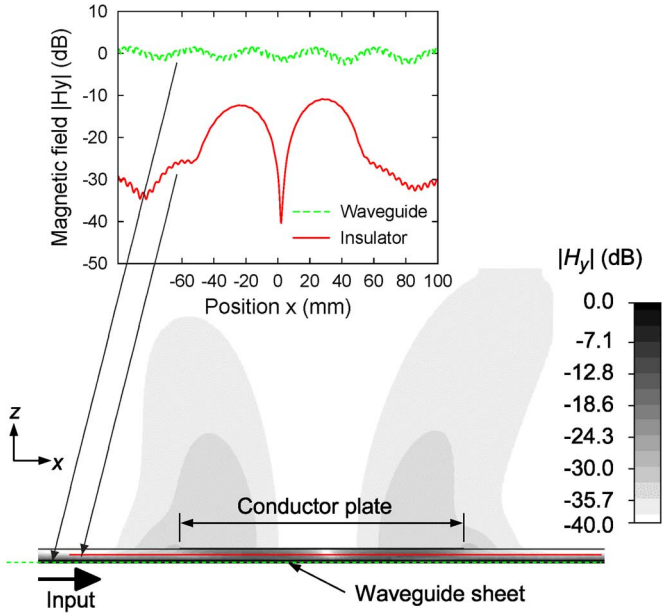

Fig. 8. Simulated magnetic field amplitude $|H_y|$ distribution map for the 101.5-mm-long conductor plate, which causes the largest power extraction in our simulation. The inset graph shows $|H_y|$ distributions along x-direction in the waveguide dielectric layer [green dashed line (in online version)] and in the surface insulator layer [red solid line (in online version)], at resonance (2.453 GHz). The average value of the magnetic field magnitude inside the sheet is set to 0 dB and the position $x = 0$ is set to the center of the conductor plate. The peak magnitude of the magnetic field inside the resonant region (-50.75 mm $\leq x \leq 50.75$ mm) in the surface insulator is 10 dB less than that in the waveguide layer.

and the other one is relatively small and gradually decays in the z-direction, as shown in Fig. 6. The former is due to the discrete structure of the mesh and the latter is due to the macroscopic reactance of the mesh [1]. In the present design, since the former significantly decays in the surface insulator layer, general objects touching the surface are not exposed to strong EM field.

In order to verify the validity of our idea, $p_{\rm ext}$ was simulated with plate lengths $D = 46 + 55.5n$ mm, where $n = 0, 1, \ldots, 9$. The shortest length, 46 mm, is determined as the shortest plate length that resonates near 2.5 GHz. The width, 55.5 mm, is nearly equal to a half wavelength in the insulator layer at 2.5 GHz. As shown in Fig. 7(a), the extraction $p_{\rm ext}$ is less than 8.5% near 2.5 GHz even in the worst case, which is a particularly rare case, and is less than 1% in usual off-resonant cases. The peak value of $p_{\rm ext}$ tends to periodically vary with respect to the conductor length, as shown in Fig. 7(b). This result agrees with our expectation described in Section III-B.

The simulated magnetic field $|H_y|$ distribution for the 101.5-mm-long plate, which is the worst (largest) extraction case, is shown in Fig. 8. The magnetic field stored in the resonant region (-50.75 mm $\leq x \leq 50.75$ mm) is 10 dB less than that in the sheet. The distribution map also shows the magnetic field from -40 to -30 dB exists outside of the resonant region and is radiated into the space. Thus, such a simple conductor plate cannot confine significantly strong EM field underneath itself and cannot extract significant power from the sheet.

The extraction can be further reduced by decreasing the mesh reactance (i.e., decreasing the mesh pitch) and/or increasing the insulator thickness. However, such changes in the sheet design

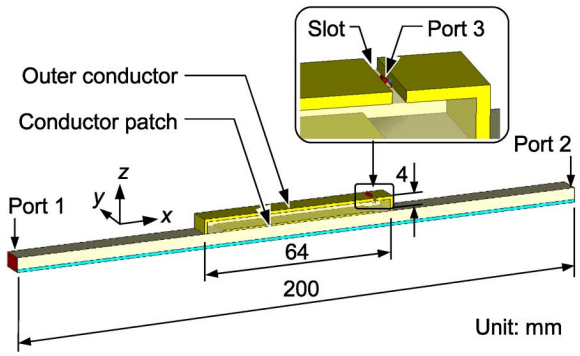

Fig. 9. Quasi-2-D simulation model of a WRR. The models have narrow width (8 mm) for the y-axis. The $\pm y$ boundary conditions are the same as those in Fig. 5. The coupler output is evaluated as the transmittance to port 3, which is set at the slot formed on the outer conductor. The impedance of port 3 is 50 Ω and the impedance matching is performed by tuning the x-offset of the slot from the center of the coupler.

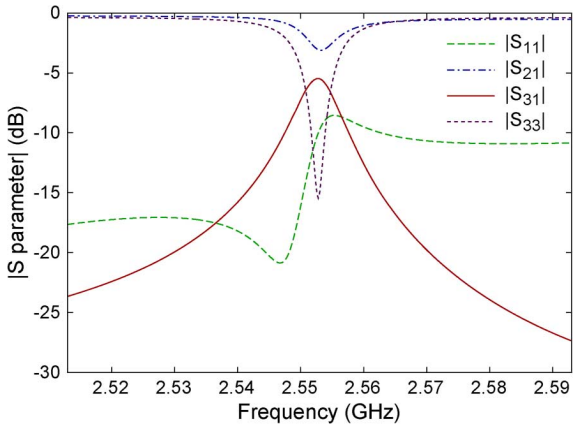

Fig. 10. Simulated S parameters. The peak value of $|S_{31}|$ is -5.47 dB at 2.553 GHz.

do not necessarily increase the selectivity because they require a higher Q of the EC coupler, which is more challenging design problem. The design parameters presented here have been determined to minimize the EM leakage under the constraint that a practical EC coupler can be designed.

V. Flat WRR Coupler

In this section, we design an EC coupler with significantly high radiation Q. The coupler designed here serves as the upper-half of the WRR, as shown in Fig. 4. The WRR has two magnetic field nodes at both ends of the coupler, as shown in the same figure. Therefore, the impedance seen looking into the WRR at the coupler ends become significantly larger than the wave impedance of the free space, and the radiation into the space will be reduced.

For approximately n-half-wavelength-long conductor plates, described in Section III, the magnetic field is also minimized at both ends of the plate. However, the simple open end does not have such impedance-boosting mechanisms, therefore the radiation loss is significant.

Fig. 9 shows the coupler simulation model, which also represents a narrow segment of the sheet and coupler. Port 1 and 2 are set at each end of the sheet, port 3, the coupler output port, is set at a slit formed on the outer conductor with a certain x-offset from the coupler center for impedance matching. The height and the relative permittivity of the coupler dielectric layer is chosen as the same as those of sheet surface insulator layer. The lengths of the conductor patch and outer conductor were determined so as to resonate near 2.5 GHz and to maximize $|S_{31}|$, and port 3 offset from the center of the coupler was determined to minimize $|S_{33}|$ through trial and error.

The simulation result is shown in Fig. 10. The peak value of $|S_{31}|$ is -5.47 dB at 2.553 GHz. Since the coupler is almost symmetric with respect to the yz-plane and $|S_{13}| \approx |S_{23}|$ (omitted in Fig. 10), the theoretical limit of the coupler output is 0.5, even if the coupler is perfectly lossless. Thus, $|S_{31}|^2 \approx 0.284$ means that 57% to the theoretical limit is achieved.

The coupler internal efficiency $\eta_{\rm int}$, defined as (5), is calculated as

$$\eta_{\rm int} \equiv \frac{|S_{31}|^2}{p_0 - (|S_{11}|^2 + |S_{21}|^2)} \approx 0.762. \tag{12}$$

where p_0 represents the value of $|S_{11}|^2 + |S_{21}|^2$ for the simulation model without a coupler. Therefore, if numbers of the same couplers are put on the sheet in a row, the total power transmission to coupler output ports from the sheet will theoretically approach 76%. The results indicate that the selectivity factor achieves about 9 (≈76/8.5).

The lost power can include the following two factors: one is the radiated power into the space and the other is the dissipated power due to the lossy materials. In the simulation model of Fig. 9, the conductivities of the mesh conductor and the coupler conductors are set to be 3.7×10^7 S/m (assuming aluminum) and 5.8×10^7 S/m (copper), respectively. The dielectric losses of the dielectrics are set to be zero.

The peak value of the magnetic field confined inside the resonant area under the coupler, shown in Fig. 11, is nearly 30 dB larger than that under the simple conductor plate, shown in Fig. 8. Moreover, such a strong magnetic field exists only inside the coupler and inside the insulator layer. The $|H_y|$ distribution map indicates that the magnetic field is less than -20 dB anywhere outside the coupler and the sheet (except around the output port 3). It means that significant power can be transferred without exposing any objects around the coupler to a significantly strong EM field. Thus, the selectivity of the system is validated in the two aspects, i.e., the selectivity factor of about 9 and the -20-dB less EM field generation outside the coupler and sheet than inside the waveguide layer.

VI. Prototype System Fabrication

In this section, we demonstrate the validity of our concept through experiments on a fabricated prototype system.

A. 3-D Structure of WRR Coupler

A schematic view of the 3-D structure and the resonant mode of the coupler is shown in Fig. 12. In the 3-D structure, the boundary condition at $\pm y$-ends of the coupler have to be considered. In the 2-D WRR resonant mode, the magnetic field vectors having opposite direction and nearly equal magnitude to each

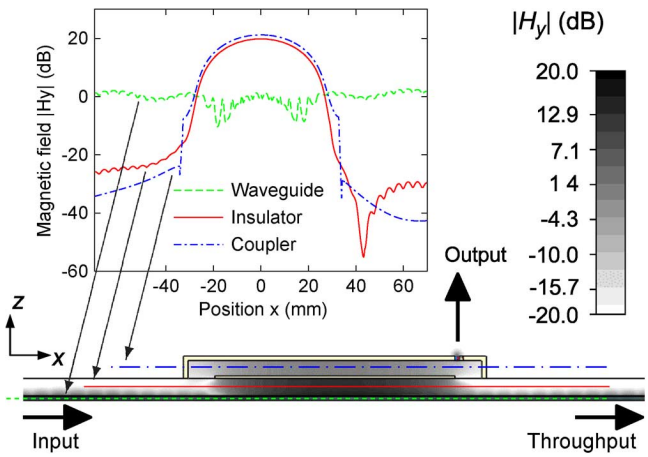

Fig. 11. Simulated magnetic field amplitude $|H_y|$ distribution map for the quasi-2-D coupler model shown in Fig. 9. The inset graph shows $|H_y|$ distributions along x-direction in the waveguide dielectric layer [green dashed line (in online version)], in the surface insulator layer [red solid line (in online version)], and in the coupler [blue dashed–dotted line (in online version)], at resonance (2.553 GHz). The average value of the magnetic field magnitude inside the sheet is set to 0 dB and the position $x = 0$ is set to the center of the coupler. The magnetic fields inside and outside the WRR region (-32 mm $\leq x \leq 32$ mm) are, respectively, 20 dB larger and 20 dB smaller than that in the sheet.

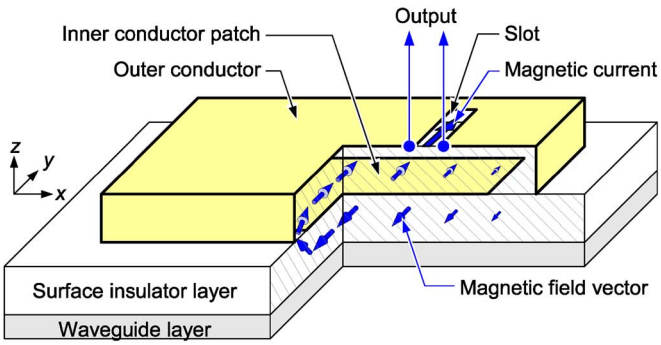

Fig. 12. Schematic view of the 3-D structure of the WRR coupler. The magnetic field vector surrounds the inner conductor patch of the coupler and lies in y-direction, except at the $\pm y$-edge of the coupler. The magnitude of the magnetic field is maximized at the center of coupler in x-direction and is minimized at the both ends. The magnetic field induces the magnetic current on the slot formed on the outer conductor for connection to the output port.

other exist in the coupler dielectric and in the sheet surface insulator. Therefore, for the 3-D structure, the inner conductor patch and the outer conductor should be separated at the $\pm y$-ends of the coupler so that the magnetic field vectors form a closed loop that surrounds the inner patch in the yz-plane.

To connect a coaxial output line, the slot is formed on the outer conductor, as shown in Fig. 12. The magnetic field in the WRR induces the magnetic current on the slot and the WRR resonant mode can couple to the coaxial line.

The design parameters of the 3-D WRR coupler are shown in Fig. 13. The patch dimensions $X_{\rm ptc}$ and $Y_{\rm ptc}$, and the outer conductor dimensions $X_{\rm out}$, $Y_{\rm out}$, and $Z_{\rm out}$ determine the resonant frequency and affect the internal efficiency. By tuning the slot dimensions $X_{\rm slt}$, $Y_{\rm slt}$ and its offset $X_{\rm ofs}$, the impedance matching between the WRR and coaxial line can be performed.

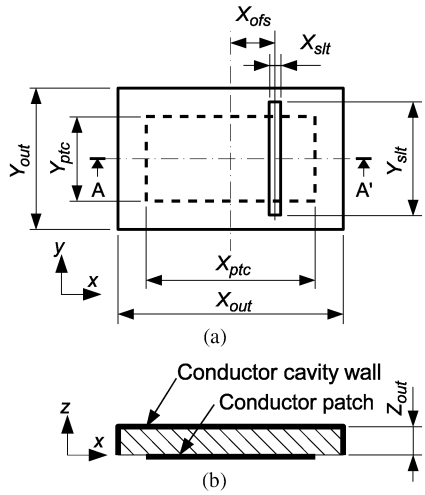

Fig. 13. Design parameters of the 3-D WRR coupler: (a) in the top view and (b) in the cross-sectional view AA'.

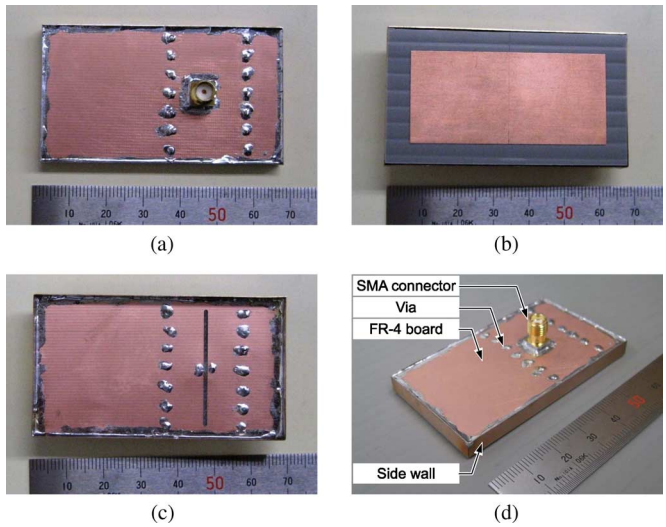

Fig. 14. One of the fabricated couplers with 36-mm width. (a) Top view, (b) bottom view, (c) bottom view without inner dielectric, and (d) perspective view. The top of the conductor cavity is copper-clad FR-4 board. The slot for WRR-to-coaxial connection is formed on inner side of the board, as shown in (c). The soldered points surrounding the slot are via connections between both sides of the board for preventing resonance in the board at the WRR resonant frequency. The sidewall and inner patch are made of 0.2-mm-thick phosphor bronze sheet and of 0.1-mm-thick copper sheet, respectively.

TABLE II
DESIGN PARAMETERS OF WRR COUPLER

X_{out}	Y_{out}	Z_{out}	X_{ptc}	Y_{ptc}	X_{slt}	Y_{slt}	X_{ofs}
64	36	4	52	24	1	30	15

The photographs and the dimensions of the fabricated coupler are shown in Fig. 14 and Table II, respectively.

A result of the simulation where the coupler is excited on a 41-mm-wide sheet is shown in Fig. 15. The magnetic field distribution along the x-axis is similar to that in 2-D simulation in Fig. 11. In the y-direction, $|H_y|$ is almost uniform inside the WRR region ($|y| \leq 12$ mm $= Y_{\rm ptc}/2$) and decays steeply near the coupler ends. Thus, the resonant mode inside the insulator layer is similar to that of a choke-enclosed coupler [12]

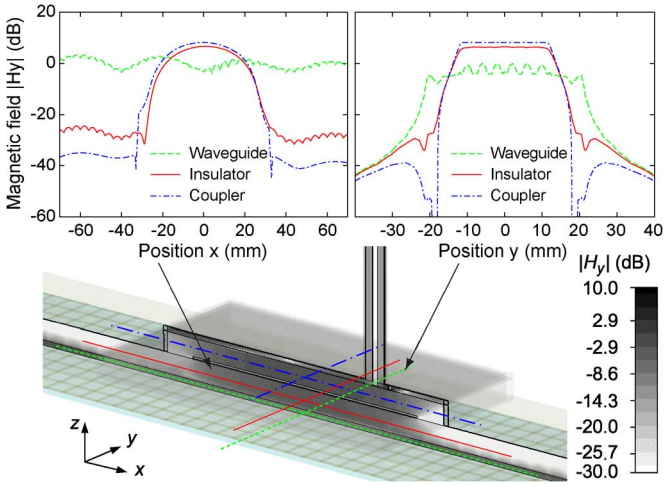

Fig. 15. Simulated magnetic field amplitude $|H_y|$ distribution map for the 3-D coupler model. The left and the right inset graphs show $|H_y|$ distributions at resonance (2.460 GHz) along x- and y-direction, respectively. Each set of the three lines represents the amplitude of the magnetic field in the waveguide dielectric layer [green dashed line (in online version)], in the surface insulator layer [red solid line (in online version)], and in the coupler [blue dashed–dotted line (in online version)], respectively. The average value of the magnetic field magnitude inside the waveguide layer is set to 0 dB and the position $x = 0$ and $y = 0$ are set to the center of the coupler. The magnetic field distribution in x-direction is similar to that in 2-D simulation result. In y-direction, $|H_y|$ in the insulator layer is almost uniform inside the WRR region and steeply decays at the edges of the coupler (around $y = \pm 15$ mm). Note that the sheet width is 41 mm in y-direction, therefore, $|H_y|$ starts to decay at $y = \pm 20.5$ mm.

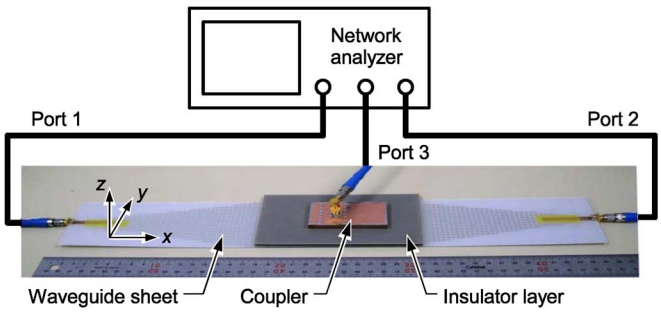

Fig. 16. Schematic diagram of the experiment setup. This graphic shows the combination of the 73-mm-wide sheet and the 36-mm-wide coupler. The sheet ends are formed as linear horns for impedance matching to the 50-Ω cables. The insulator layer covers the center area of the sheet.

because the "open-end" boundary condition at the coupler circumference is common for them. The coupler does not generate significantly strong EM field outside of the coupler and sheet also in the 3-D model.

B. S-Parameter Measurement on Experimental Setup

The experimental setup is shown in Fig. 16. The sheet design parameters follow those in the simulation shown in Table I. Alminum/PET laminated sheets are used for the ground plane and mesh conductor plane. The mesh pattern is the same as that in the simulation. The dielectric waveguide layer is a 1-mm-thick polypropylene (PP) sheet and has a relative permittivity of 2.1. The insulator layer is a 4-mm-thick hollow sheet made of PP, whose cross section is shown in Fig. 2(a). The volume filling factor is approximately 15% and the effective relative permittivity is estimated to be 1.17, which equals that in simulation.

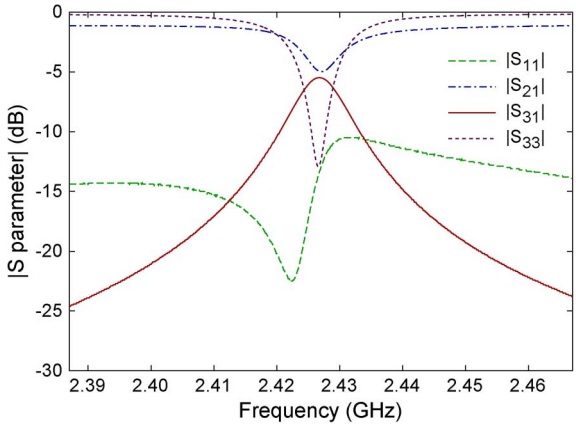

Fig. 17. Measured S-parameters for the combination of the 41-mm-wide sheet and the 36-mm-wide coupler. Transmittance $|S_{31}|$ is maximized at 2.427 GHz and achieves -5.49 dB.

TABLE III
MEASUREMENT RESULT SUMMARY

Sheet width (mm)	Coupler width (mm)	$\lvert S_{31max}\rvert$ (dB)	Q_{ext}	η_{int}	Resonant frequency (GHz)
41	21	-7.84	381	51.3%	2.477
	36	-5.49	258	63.1%	2.427
73	21	-9.18	419	54.3%	2.472
	36	-6.92	303	67.9%	2.425

The sheet width is 41 mm, the same as the simulation model shown in Fig. 15. Although the power transmission using such a narrow and resistance-terminated (i.e., connected to 50-Ω port and the throughput power is absorbed) sheet is not a practical situation for 2-D power transmission, it is reasonable for the fundamental coupler characteristics evaluation.

The S-parameters were measured by network analyzer E5071C, Agilent Technologies Japan Ltd., Tokyo, Japan. The measured result is shown in Fig. 17. The maximum $|S_{31}|$ achieves -5.49 dB, which means 28.3% of the power fed into the sheet is extracted, as shown in Fig. 17. In this case, the theoretical limit of the output of the lossless coupler that is symmetric with respect to the yz-plane is 0.5. Thus, the produced coupler achieves the performance of 57% to the theoretical limit. The internal efficiency is calculated as (12), where p_0 represents $|S_{11}|^2 + |S_{21}|^2$ for the setup without the coupler, and $\eta_{\rm int} \approx 0.631$ is derived. Measurement results including combinations of another coupler width and another sheet width are summarized in Table III.

VII. POWER TRANSMISSION DEMONSTRATION

In this section, we demonstrate the applicability of the coupler to a practical situation where several couplers operate on a large sheet simultaneously. The output power of each coupler is measured on an experimental setup shown in Fig. 18, which is similar to one shown in Fig. 1. The sheet dimensions are 90 cm $\times$ 60 cm and its circumference is open ended. Each coupler is loaded with a 50-Ω chip resister and the terminal voltage of the load is rectified and measured by using an ADC, Contec

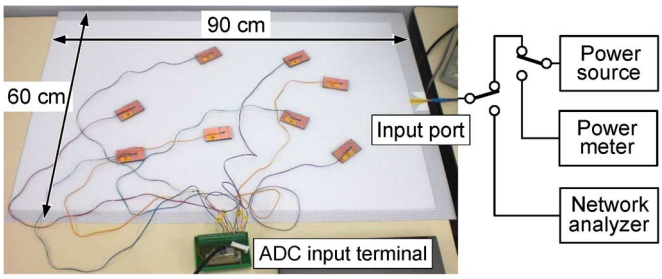

Fig. 18. Experiment setup for measurement of the power transferred to eight couplers. Each coupler output is rectified by the rectifying circuit embedded onto the coupler and the rectified voltage is conducted to the ADC input terminal by a parallel pair cable. The return loss at the sheet input port is measured by a network analyzer, while the coupler positions keep being unmoved. The power source output is measured by the power meter.

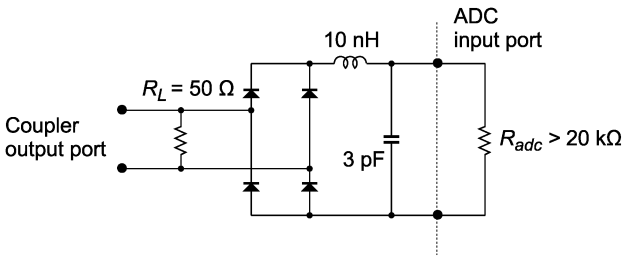

Fig. 19. Circuit connected between the coupler output port and the ADC input port. While the RF voltage appear between the resistor terminal pair, the voltage rectified and smoothed through the diodes and the *LC* filter is measured through the ADC input port.

AD12-8(PM). The rectifying circuit is shown in Fig. 19. The diodes used in the circuit are Toshiba 1SS295.

The power consumption P_R at the load is estimated as follows:

$$P_R = \frac{1}{2}\frac{(V_{\rm adc} + 2V_f)^2}{R_L} \tag{13}$$

where $V_{\rm adc}$, V_f, and R_L represent the voltage measured by the ADC, forward voltage drop of the diode, and load resistance, respectively. V_f is estimated as follows:

$$V_f = c_1 \ln c_2 I_f \tag{14}$$

where I_f represents the forward current of the diode. Coefficients c_1 and c_2 are determined by curve fitting to the $I_f - V_f$ curve in the datasheet of the diode. The fitted curve well approximates the $I_f - V_f$ curve in the region of $I_f < 1$ mA. Note that $V_{\rm adc}$ ranges from 1 to 4 V, and I_f is estimated to be less than 1 mA in the experiments. Current I_f is estimated as $V_{\rm adc}/R_{\rm adc}$, where $R_{\rm adc}$ represents the input impedance of the ADC. According to the datasheet of the ADC, $R_{\rm adc}$ is larger than 20 kΩ. Here we assumed $R_{\rm adc} = 100$ kΩ for cautious estimation.

Table IV shows the estimated coupler output powers and the loss. The loss in Table IV is calculated by subtracting all of the coupler outputs from the input power to the sheet. The input power is calculated by subtracting the reflected power from the power source output (427 mW) measured by the power meter (Agilent E4418B). The reflected power is calculated from the return loss (−17.2 dB) measured by the network analyzer.

TABLE IV
EIGHT COUPLER OUTPUTS AND LOSS

Number	1	2	3	4	5	6	7	8	Loss
Wattage (mW)	52.4	52.4	51.5	47.8	43.9	41.3	40.5	37.6	51.5

In this case, the microwave transmission efficiency is calculated to be 87.7%, which is higher than the internal efficiency of the single coupler operation measured in Section VI. Such improvement in overall efficiency by multiple receivers is also reported in another study based on resonant inductive coupling [16].

That is the best result found in searching the best positions of the couplers, where the outputs are maximized, by moving the couplers around on the sheet. Each coupler output depends on the position of itself and also on the positions of other couplers, all of which affect the amplitude distribution of EM standing wave in the sheet. The results demonstrate that the coupler designed here is potentially applicable to a practical large-area 2DWPT.

VIII. CONCLUSION

In this paper, we showed a design procedure of a selective 2DWPT system. The system requires significantly high Q to extract power out of the sheet and prevents general objects from such high-Q resonance.

The simulation results shows that the accidental power extraction rate is less than 8.5% even in the worst case, which is a particularly rare case, and is less than 1% in general off-resonant cases. We also designed a receiver coupler that works on such a sheet. The simulated coupler internal efficiency is 76.2% for the 2-D reduced model. The selectivity factor $9 \approx 76.2/8.5$ is the highest value we found in trial and error, however, this is not the theoretical limit. Since the design is restricted by characteristics of available materials, the selectivity factor can increase if more efficient materials become available. Developing an alternative coupler with higher unloaded Q also contributes to improving the selectivity and is the subject of future study.

The measured internal efficiency of the prototype coupler achieved 67.9%, which agrees well with the simulation result. Coupler operation on a large (90 cm × 60 cm) sheet was also demonstrated and 87.7% efficiency (from microwave input to microwave output) was achieved at a maximum by eight couplers. This result proves that such a high-efficiency power transmission is possible on the condition that the coupler positions are adjusted to the appropriate positions. Developing a more stable power transmission system insensitive to the coupler positions is also one of the future studies.

ACKNOWLEDGMENT

Some materials for the waveguide sheet were provided by Teijin Fibers Limited, Osaka, Japan.

REFERENCES

[1] H. Shinoda, Y. Makino, N. Yamahira, and H. Itai, "Surface sensor network using inductive signal transmission layer," in *Proc. 4th Int. Networked Sensing Syst. Conf.*, Jun. 2007, pp. 201–206.

[2] A. Noda and H. Shinoda, "Power transmission coupler for low leakage 2D-communication sheet," in *Proc. 6th Int. Networked Sensing Syst. Conf.* , Pittsburgh, PA, Jun. 2009, pp. 24–30.
[3] A. Noda and H. Shinoda, "The lower-bound of electromagnetic leakage of 2-D wireless power transmission," in *Proc. 7th Int. Networked Sensing Syst. Conf.*, Kassel, Germany, Jun. 2010, pp. 138–144.
[4] W. C. Brown, "The history of power transmission by radio waves," *IEEE Trans. Microw. Theory Tech.*, vol. MTT-32, no. 9, pp. 1230–1242, Sep. 1984.
[5] A. Sample and J. R. Smith, "Experimental results with two wireless power transfer systems," in *Proc. IEEE Radio Wireless Symp.*, 2009, pp. 16–18.
[6] T. Ungan, M. Freunek, M. Müller, W. D. Walker, and L. M. Reindl, "Wireless energy transmission using electrically small antennas," in *Proc. IEEE Radio Wireless Symp.*, 2009, pp. 526–529.
[7] A. Kurs, A. Karalis, R. Moffatt, J. D. Joannopoulos, P. Fisher, and M. Soljačić, "Wireless power transfer via strongly coupled magnetic resonances," *Science*, vol. 317, pp. 83–86, 2007.
[8] T. Sekitani, M. Takamiya, Y. Noguchi, S. Nakano, Y. Kato, T. Sakurai, and T. Someya, "A large-area wireless power-transmission sheet using printed organic transistors and plastic MEMS switches," *Nature Mater.*, vol. 6, pp. 413–417, Apr. 2007.
[9] E. Waffenschmidt and T. Staring, "Limitation of inductive power transfer for consumer applications," in *Proc. 13th Eur. Power Electron. Appl. Conf.*, 2009, pp. 1–10.
[10] B. Zhang, A. O. Lim, Y. Kado, H. Itai, and H. Shinoda, "An efficient power supply system using phase control in 2-D communication," in *Proc. 6th Int. Networked Sensing Syst. Conf.*, Pittsburgh, PA, Jun. 2009, pp. 110–113.
[11] K. Eom and H. Arai, "Wireless power transfer using sheet-like waveguide," in *Proc. 3rd Eur. Antennas Propag. Conf.*, Berlin, Germany, Mar. 2009, pp. 3038–3041.
[12] A. Noda and H. Shinoda, "Selective wireless power transmission through 2-D waveguide sheet using strong electromagnetic confinement by choke-enclosed resonant coupler," in *Proc. IEEE Radio Wireless Symp.*, Phoenix, AZ, Jan. 2011, pp. 178–181.
[13] International Commission on Non-Ionizing Radiation Protection, "Guidelines for limiting exposure to time-varying electric, magnetic, electromagnetic fields (up to 300 GHz)," *Health Phys.*, vol. 74, no. 4, pp. 494–522, 1998.
[14] N. Kobayashi, H. Fukuda, and T. Tsukagoshi, "Challenging EMC problems on two-dimensional communication systems," in *Proc. 7th Int. Networked Sensing Syst. Conf.*, Jun. 2010, pp. 130–137.
[15] A. Yariv, "Critical coupling and its control in optical waveguide-ring resonator systems," *IEEE Photon. Technol. Lett.*, vol. 14, no. 4, pp. 483–485, Apr. 2002.
[16] A. Kurs, R. Moffatt, and M. Soljačić, "Simultaneous midrange power transfer to multiple devices," *Appl. Phys. Lett.*, vol. 96, no. 4, pp. 044 102–044 102-3, 2010.

Akihito Noda (S'10) received the B.E. degree in control and systems engineering from the Tokyo Institute of Technology, Tokyo, Japan, in 2005, the M.E. degree in information physics and computing from the University of Tokyo, Tokyo, Japan, in 2010, and is currently working toward the Ph.D. degree at the University of Tokyo.

From 2005 to 2008, he was an Engineer with INCS Inc. He is currently a Research Fellow with the Japan Society for the Promotion of Science (JSPS). His current research interest includes WPT technology.

Mr. Noda is a member of the Institute of Electronics, Information and Communication Engineers (IEICE), Japan, and the Society of Instrument and Control Engineeres (SICE), Japan.

Hiroyuki Shinoda (M'10) received the B.S. degree in applied physics, M.S. degree in information physics, and Doctoral degree in electrical engineering from the University of Tokyo, Tokyo, Japan, in 1988, 1990, and 1995, respectively.

In 1995, he was a Lecturer and in 1997, he was an Associate Professor with the Department of Electrical and Electronic Engineering, Tokyo University of Agriculture and Technology, Tokyo, Japan. In 1999, he was a Visiting Researcher with the University of California at Berkeley. Since 2000, he has been an Associate Professor with the Graduate School of Information Science and Technology, University of Tokyo. His research interests include information physics, tactile/haptic interfaces, sensor systems and devices, sensor networks, 2-D communication, human interfaces, and optical/acoustic measurement.

Dr. Shinoda is a member of the Institute of Electrical Engineers of Japan (IEEJ), the Robotics Society of Japan (RSJ), Virtual Reality Society of Japan (VRSJ), and the Japan Society of Mechanical Engineers (JSME). He was a board member of he Society of Instrument and Control Engineeres (SICE), Japan, in 2008 and 2009. He and his students were the recipients of six international conference awards, excluding two finalists and many Japanese academic awards.